European Polymer Journal 157 (2021) 110642

Contents lists available at ScienceDirect

European Polymer Journal

journal homepage: www.elsevier.com/locate/europolj

Engineered PP impact copolymers in a single reactor as efficient method for determining their structure and properties

María Teresa Pastor-García, Inmaculada Suárez, María Teresa Expósito, Baudilio Coto, Rafael A. García-Muñoz *

ESCET, Universidad Rey Juan Carlos, 28933 Móstoles, Madrid, Spain

ARTICLE INFO

Keywords:
Impact polypropylene copolymers
IPCs synthesis
Ziegler–Natta catalyst
Polyolefins' characterization
Impact resistance

ABSTRACT

Impact polypropylene (PP) copolymers (IPCs) are important materials for many commercial applications. These materials are usually synthetized through different methods involving two consecutive reactions in the same phase or in different phases. Here, a laboratory-scale synthesis method based on a sequential liquid- and gas-phase two-step process in a single reactor is developed. Propylene homopolymers and IPCs were synthesized with varying amounts of comonomers and hydrogen. The IPC materials obtained were fully characterized via analytical temperature rising elution fractionation (TREF), differential scanning calorimetry (DSC), ^{13}C nuclear magnetic resonance (^{13}C NMR), gel permeation chromatography with an infrared detector (GPC-IR5), Charpy impact, scanning electron microscopy (SEM), and cross-fractionation chromatography (CFC). The addition of only ethylene to the second step in the absence of hydrogen led to the creation of an ethylene-propylene (EP) copolymer with similar impact strength to that of a propylene homopolymer. The addition of hydrogen to the first step dramatically shortened the length of the PP chains and inhibited catalytic active centers that led to EP copolymer synthesis. This material exhibited very low molecular weight, low ethylene incorporation, and rubbery phases irregularly distributed along the isotactic polypropylene (iPP) matrix, resulting in the formation of an EP copolymer material with poor impact properties. IPCs synthesized without hydrogen and with a 50/50 (v/v) mixture of propylene/ethylene monomers in the second step enhance ethylene incorporation, facilitating adequate homogeneous and heterogeneous ethylene distribution and resulting in a high increment of amorphous ethylene-propylene-rubber (EPR) domains, which remarkably improves impact properties. Additionally, a criterion based on the ratio between EEE and EPE + PEP triads ranging between 1 and 2 was also established to predict the impact resistance of any heterophasic PP. Fractionation of the optimal sample provided a detailed understanding about the microstructure of this copolymer through the study of the molecular weight and composition of the fractions via GPC-IR, analytical TREF, and DSC measurements. Finally, the liquid–gas-phase two-step IPC material was compared, by means of SEM and CFC measurements, with synthesized IPC using liquid–liquid-phase two-step polymerization, and the results showed that the range of EP composition as well as ethylene distribution in the molar mass molecules of the IPCs was correlated to their mechanical behavior. This proves that crystalline families composed of high-molecular-weight EP copolymers in the liquid–gas-phase process can act as a compatibilizing agent between the iPP matrix and the elastomeric rubbery phase, allowing one to improve the impact resistance of the IPC, more so than that of IPCs obtained in the gas–gas and liquid–liquid phases. The results indicate that the synthesis of IPC resins in a single reactor is an efficient experimental method for fundamental research on IPCs.

1. Introduction

The discovery of the Ziegler–Natta (Z–N) catalyst in the 1950s significantly impaired the production of polyolefins incorporating different chain microstructures and properties and since then has continuously grown with the rapid development of catalyst technology combined with polymerization innovation [1,2].

Polypropylene (PP) is one of the most important materials among polyolefins for three main reasons. First, PP holds remarkable properties such as low density, high melting temperature, and chemical inertness

* Corresponding author.
E-mail address: rafael.garcia@urjc.es (R.A. García-Muñoz).

https://doi.org/10.1016/j.eurpolymj.2021.110642
Received 24 April 2021; Received in revised form 3 July 2021; Accepted 6 July 2021
Available online 8 July 2021

with low cost, which make PP optimal for long-life applications. Second, PP is a highly versatile material, meaning that diversity in structural designs and mechanical properties is achievable. Third, different morphological structures of PP are available via fillers or reinforcing agents and the blending of PP with other polymers that yield materials with superior features [3,4]. However, isotactic polypropylene (iPP), as is well known, has extremely poor low-temperature impact properties, and therefore, several approaches to improve its toughness have been implemented, such as blending with elastomers and copolymerizing with α-olefinic moieties [5–7]. Other methods are developed at the industrial scale, especially in situ copolymerization with ethylene by means of sequential gas- and liquid-phase reactors in the production line, which is proven to be extremely effective to obtain high-impact-resistant PP, commonly referred to as impact PP copolymers (IPCs) or high-impact PPs (HIPPs) [8].

IPCs combine a crystalline iPP matrix (produced in the first one or two reactors) with embedded particles of ethylene-propylene-rubber (EPR) and polyethylene segments (incorporated in the sequentially following reactors) defining impact and low-temperature resistance [9]. Therefore, IPCs are alloys of PP and ethylene-propylene (EP) copolymers of varying ethylene content with an array of block lengths [10]. The amorphous copolymer fraction is responsible for increasing the impact strength of the homopolymer matrix formed in the first reactor [11]. Toughening efficiency has been associated with rubber content, morphological structure, phase composition, particle shape, particle size, size distribution, viscosity, and rubber–matrix compatibility [12–18]. These materials have high impact resistance and have applications in the consumer and automotive industries [19–22].

On the industrial scale, the Spheripol process offers licenses a simple and economical method of producing a wide range of PP products of the highest quality. This product range can be expanded easily. These plants offer on a single polymerization line the widest range of homopolymers, random copolymers, and terpolymers as well as heterophasic impact copolymers covering all PP applications fields [23]. In the Spheripol process (Basell), two loops are used in a series to narrow the residence time distribution of the catalyst particles. The liquid propylene/polymer suspension from the first stage is flashed to gas/solid conditions prior to entering the second stage. Then the particles are transferred to a continuous gas-phase fluidized bed reactor where the elastomeric phase is produced within the iPP. The properties of a HIPP mainly depend on particle morphology, which, in turn, depends on both the catalyst and the process conditions [24].

Laboratory-scale hybrid technologies have been developed to study the influence of synthesis variables on material properties. Polymers are synthesized through a combination of both types of reactors in a two-stage reaction process, homopolymerization in liquid propylene, and, in the second stage, successive gas-phase EP copolymerization in a stirred-bed reactor [25]. These materials have also been synthetized in only one reactor using a multistage subsequential polymerization process, in slurry in the first stage and with n-heptane and EP gas in the second stage, with discharge during the process to keep the composition constant [26,27]. Thus, slurry and gas are used for synthesizing IPC materials [28,29].

The main objective of this study is to develop an alternative approach for engineering IPC materials in only one reactor for laboratory-scale research to emphasize the importance of experimental variables in IPC synthesis and their influence on IPC structure and properties. This method is based on a sequential liquid- and gas-phase two-step process but in a single reactor using a Z–N catalyst. Process variables such as the addition of hydrogen, the amount of ethylene and propylene, and the pressure and time of monomer additions have been studied, and the morphological characteristics of IPC materials were compared with those obtained in the liquid–liquid-phase [30] and gas–gas-phase processes [31]. Mechanical performance was obtained from notched Charpy impact strength. Thermal properties in the solution and in the solid state were determined via temperature rising elution fractionation (TREF) and differential scanning calorimetry (DSC). Two-dimensional distribution interrelating molar mass and chemical composition to acquire full bivariate distribution was determined via cross-fractionation chromatography (CFC). The molecular microstructure was acquired via liquid-state ^{13}C nuclear magnetic resonance (^{13}C NMR) and gel permeation chromatography (GPC-IR5). Finally, the morphology and distribution of the EPR phase in the iPP matrix were determined via scanning electron microscopy (SEM) for the required comprehensive characterization of these complex materials.

2. Experimental method

2.1. Materials

Propylene, ethylene, and hydrogen were supplied by Praxair SA (99.99%) and the solvent n–heptane by Scharlab SA (99%). All the polymers were synthetized using a standard $TiCl_4/MgCl_2$ Z–N catalyst containing 2.5 wt% Ti, triethylaluminum was used as a cocatalyst and scavenger (TEA 1 M in n–heptane, supplied by Witco), and cyclohexylmethyldimethoxysilane (C–donor, Wacker Química Ibérica SA) was used as an external donor [32]. Sodium chloride used for every experiment in the gas phase was supplied by Scharlab SA.

2.2. Synthesis procedure

A schematic drawing of the experimental setup is shown in Fig. 1a.

In this procedure, IPCs have been synthesized in two sequential liquid- and gas-phase steps using one 2 L autoclave stirred reactor. A jacketed steel vessel allowed for heating the reaction volume with a water bath by a thermostat (Julabo), and a coil placed inside the reactor allowed for refrigeration by cool water. This system is used to control the temperature at 70 °C for all the runs. Monomers were fed through calibrated gas flowmeters supplied by Bronkhorst Hi-Tec. To accomplish this sequential reaction, a helical stirrer (previously described) [31] and an extraction system are placed for emptying the reactor through an outlet at the bottom of the reactor (Fig. 1a) with a mesh to prevent the movement of the polymer out of the reactor. A cooling system to allow internal refrigeration was implemented and previously described [31].

The polymerization procedure requires two different steps, as shown in Fig. 1b: (1) propylene homopolymerization (pre-polymerization and main polymerization) and (2) EP copolymerization. In this work, propylene homopolymers and IPCs were synthesized at varying amounts and times of addition of monomers, pressures, and hydrogen. Propylene, ethylene, and n-heptane were deoxygenated and dried through columns containing a R-3/15 BASF catalyst, alumina, and 3 Å molecular sieves before being fed to the polymerization reactor.

The solvent (400 mL of n-heptane) was introduced into the reactor and was saturated with propylene at pre-polymerization conditions described in a previous work [30]. This stage was maintained for 17 min. Then the temperature was raised to 70 °C, and the desired amount of hydrogen was added according to Fig. 1b as the start of the main polymerization stage. The PP matrix synthesis stage in the liquid phase was maintained for 60 min, and the propylene monomer was fed to keep the pressure at 8 bars. The solvent was carefully removed before the next gas-phase step to avoid the loss of synthesized PP and without stopping the reaction and opening the reactor to prevent catalyst deactivation. A solvent extraction time of 15 min was set up to generate reproducible results and for comparison purposes. Solvent extraction occurred at the bottom of the reactor by means of pressure difference, while stirring was maintained to avoid polymer deposition. Inert sodium chloride (60 g) was used for every experiment to prevent the polymer particles from sticking to one another and to the reactor wall during the gas-phase stage. Sodium chloride also improved the heat transfer from the reacting particles to the reactor wall [33,34], was calcined at 150 °C for 24 h, and was introduced in the reactor with overpressure of N_2.

After the first step, the reactor was vented several times with N_2, and

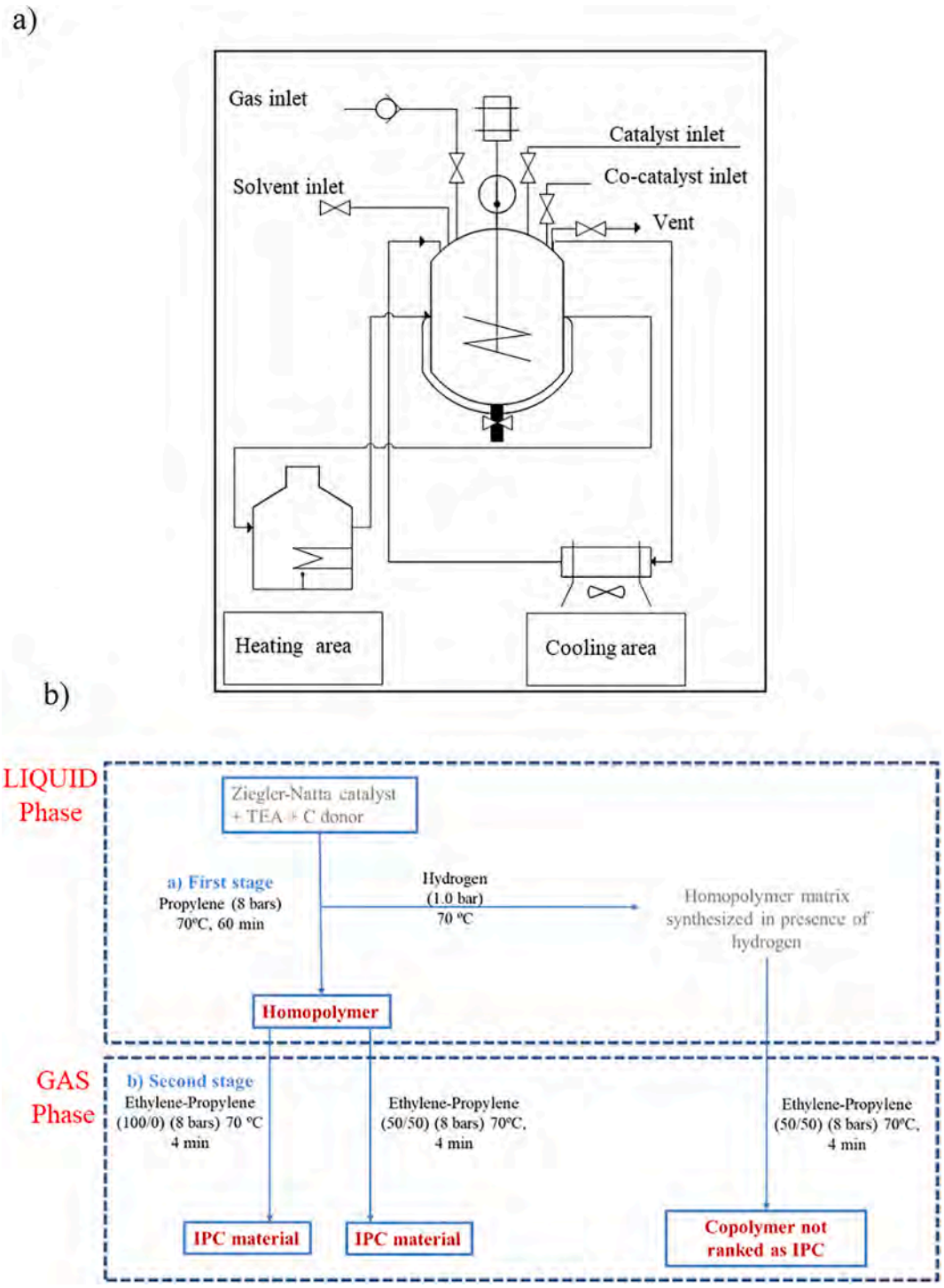

Fig. 1. (a) Scheme of polymerization reactor, and (b) scheme of reaction process in two sequential liquid- and gas-phase steps.

stirring was maintained to ensure the complete removal of unreacted propylene, hydrogen, and residual solvent. Then an ethylene monomer or a 50/50 (v/v) mixture of propylene/ethylene monomers was fed at 8 bars for 4 min, as shown in Fig. 1b. After the polymerization reaction, the polymers were washed with water to dissolve the sodium chloride, and they were recovered via filtration and dried.

2.3. Characterization of samples

The samples were characterized using different techniques. GPC-IR5 (7890A Polymer Char) was used to determine the average molecular weights (M_w and M_n), molecular weight distributions (MWDs), and polydispersity indices using three columns (PLgel Olexis of Agilent). The conditions for these analyses were a temperature of 160 °C, a flow rate of 1.0 mL·min^{-1}, and 1,2-dichlorobenzene as a solvent. This GPC instrument also records the content of methyl groups as CH_3/1000 total carbons or as a function of molar mass.

DSC (Mettler-Toledo 822e) equipped with a liquid nitrogen sub-ambient accessory was used for thermal analysis. Melting and crystallization thermograms were recorded by heating the samples in three steps: from −100 °C to 250 °C, followed by cooling from 250 °C to −100 °C and reheating again to 250 °C at rates of 10 °C·min^{-1}. The

melting point and crystallization degree values were taken from the second heating scan. The equilibrium melting enthalpy of a PP infinite crystal was taken as 482 J g^{-1}.

The monomer composition and triads distribution values were determined via ^{13}C NMR. The samples were solved in TCB and d^6-*ortho*-dichlorobenzene and analyzed at 100 °C on a Bruker DRX 500 spectrometer operating at 75.4 MHz, and an assignment of chemical shift was carried out according to Randall [35] and Kakugo [36].

The powder samples were compression-moulded to a 4 mm plaque using a hydraulic press at 180 °C and a nominal pressure of 50 bars, with a cooling rate of 15 °C/min. Charpy specimens of 4 × 10 × 80 mm (thickness × width × length) were machined from the plaque. A V-notch of 45°±1° and a root radius of 0.25 ± 0.05 mm was made via sawing with a razor. The Ceast Charpy impact tester allows one to obtain impact measurements, which were performed at 23 °C to determine the fracture mechanics values as resistance according to UNE-EN ISO179-1:01/A1:05. The impact speed was always 2.9 m·s^{-1}.

The analytical TREF experiments were carried out in a CRYSTAF-TREF 200+ (PolymerChar, Spain) equipped with five separate crystallization vessels for the sequential or simultaneous analysis of five different polymeric samples. In addition, 80.0 ± 0.5 mg of the polymer were dissolved in TCB with 300 ppm of antioxidant 2,6-di-tert-butyl-4-methylphenol (BHT) at 160 °C for 60 min at a concentration of 4 g·mL^{-1}.

CFC was performed in a fully automated Polymer Char instrument. Two-dimensional distribution relating to molar mass and composition distribution are obtained. The PP samples are placed (40 mg) into disposable vials, which are brought to the autosampler tray. The instrument automatically fills the vials with o-DCB and dissolves them at temperatures of 140 °C for 90 min. The polymer solution (2 mg/mL) is loaded into the TREF column, where it is crystallized by cooling down the TREF oven from 140 °C to 30 °C at 0.5 °C/min and subsequently eluting the fractions in stepwise temperature increments, from 30 °C to 140 °C, toward the GPC columns. The instrument fractionates polymers according to crystallinity in 28 fractions, which are continuously injected toward online GPC columns where a second round of fractionation, this time according to molar mass, is performed.

The iPP_l-$4EP_g$ sample was divided into three fractions (F1, F2, and F3) using a preparative fractionation PREP mc2 instrument (Polymer Char) in TREF mode. The polymer (1.5 g) was dissolved in 100 mL of xylene at 130 °C under stirring. The mixture was cooled to 95 °C, kept at this temperature for 45 min, and then cooled gradually to 50 °C at 0.1 °C·min^{-1}. The first fraction (F1) was obtained at 50 °C. Then the temperature was raised in different steps at 100 °C and 130 °C to gather the rest of the fractions. A volume of 200 mL of each fraction was collected in a beaker. These fractions were further precipitated in acetone, filtrated, and dried under vacuum.

The morphology of polymer particles and dispersion of the EPR phase in the iPP matrix were studied using an environmental scanning electron microscope (XL 30 ESEM, Phillips). The SEM samples to analyze EPR dispersion were prepared by cutting them in liquid nitrogen by ultramicrotome, and their surfaces were dipped into and etched by n-heptane under ultrasonic at 60 °C for 60 min. An operating voltage of 22.0 kV was used to observe the surfaces of the samples after coating them with gold. The counts of EPR particles were determined using image analysis software (Digital Micrograph version 3.6.5).

3. Results

Table 1 compiles the synthesized resin samples. The homopolymer was named as an iPP with a subscript liquid phase (l). Three different IPC resins were synthesized in this work: an IPC material with only an ethylene monomer (E) incorporated in the second step for 4 min (iPP_l-$4E_g$); an IPC resin with a mixture of ethylene and propylene (EP) (50% each) also incorporated in the second step for 4 min (iPP_l-$4EP_g$); and an IPC copolymer similar to iPP_l-$4EP_g$ but with the addition of hydrogen for 1 min at the first step (iPP_l-1.0-$4EP_g$). Also, an IPC resin, iPP_l-$1E_l$, previously synthesized in the liquid–liquid phase in two steps, was used for comparison. Fig. 1b displays the experimental conditions for the synthesis of all the materials. Likewise, Figs. 2, 3, 4, and 5 show the GPC, TREF, DSC, and SEM results, respectively, of the PP homopolymer and synthesized IPC resins.

3.1. Effect of ethylene addition on IPCs

PP homopolymerization to obtain iPP_l was performed in the liquid phase. This involved polymerization for 60 min at 8 bars and 70 °C. To generate IPC materials, the second-step polymerization process was performed by adding an ethylene comonomer to the reactor for 4 min at the conditions displayed in Fig. 1b to generate EPR elastomeric domains embedded in the iPP matrix. Table 1 shows the activity expressed as $g_{polym}·g^{-1}{}_{cat}·min^{-1}$ and the characterization results of the propylene homopolymerization (sample iPP_l) and IPC resin (sample iPP_l-$4E_g$ and iPP_l-1.0-$4EP_g$). The activity values in the second gas-phase step are lower than those obtained in the liquid phase excepting the polymerization in the presence of hydrogen, in agreement with the previous results [30,31].

A ^{13}C NMR analysis of the sample iPP_l-$4E_g$ (presented in Table 1) determined a total ethylene molar percentage of 4.5 mol%, with a heterogeneous distribution, quantified by EEE triad mol%, of 3.9% and a

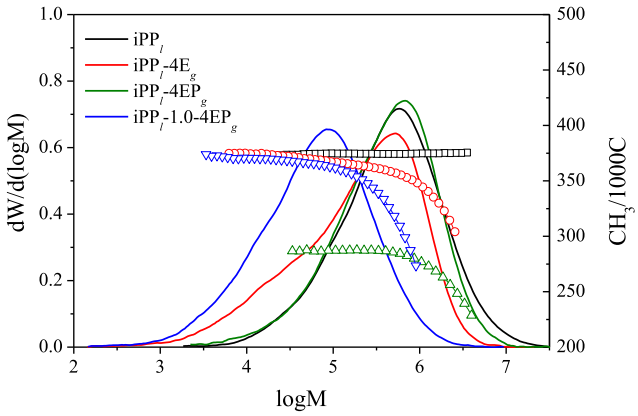

Fig. 2. Molecular weight and methyl group distributions determined from GPC of PP homopolymer and IPC resins.

Table 1
GPC, DSC and ^{13}C NMR results of PP homopolymer and IPCs materials.

Sample	Productivity $g_{polym}·g^{-1}cat·min^{-1}$	M_w (kg/mol)	PI	T_m (°C)	T_g (°C)	Crystallinity (α, %)	MFI (g/10 min)	Charpy impact (kJ·m^{-2})	P (% mol)	E (% mol)	EPE + PEP (% mol)	EEE (% mol)
iPP_l	36.7	1122.1	6.9	163.0	−5.5	46	0.35	8.0 ± 0.6	100	0.0	0.0	0.0
iPP_l-$4E_g$	11.7	981.7	5.2	162.0	−5.5	54	0.15	7.6 ± 0.9	95.5	4.5	0.1	3.9
iPP_l-$4EP_g$	23.4	806.7	6.5	115.9/162.8	−56.3	25	0.05	13.8 ± 1.7	78.7	21.2	6.3	12.2
iPP_l-1.0-$4EP_g$	42.8	153.4	9.5	119.3/160.5	−9.4	57	56.10	1.8 ± 0.7	95.5	4.5	1.8	2.6

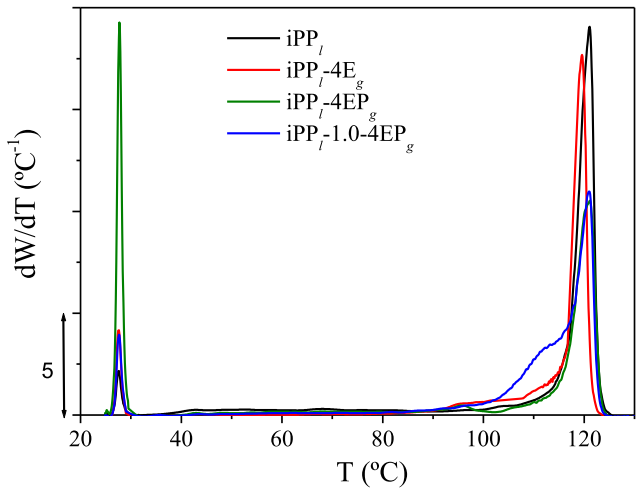

Fig. 3. Compositional distribution determined by TREF of PP homopolymer and IPC resins.

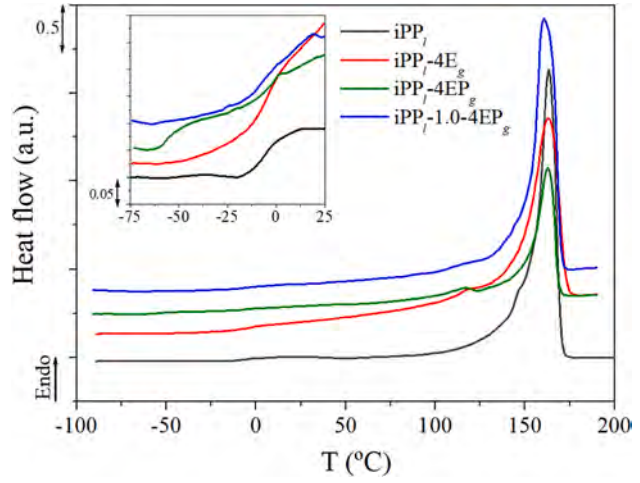

Fig. 4. Melting thermograms obtained from the second heating scanning determined by DSC of PP homopolymer and IPC resins.

homogeneous distribution, PEP + EPE mol%, of around 0.1%. This result indicates the formation of long ethylene sequences with the capability to crystallize and an almost negligible presence of elastomeric EPR chains. The lower molecular weight of iPP$_l$-4E$_g$ compared with that of iPP$_l$ (Table 1 and Fig. 2) and the variation of the content of methyl branches with molar mass shown in Fig. 2 suggest that a propylene comonomer is incorporated into the lower molar mass molecules and an ethylene comonomer is added in the higher molar mass chains during the gas-phase step. Additionally, in the MWD of the iPP$_l$-4E$_g$ resin, a shoulder of lower molar mass is observed that can be associated with those chains composed mainly of propylene since the methyl branch content (Fig. 2) at this low molecular weight is around 400 CH_3/1000C, which matches well with that of the iPP$_l$ homopolymer. As a consequence, the crystallinity degree becomes higher than that of the iPP$_l$ sample (Table 1).

The TREF thermogram (Fig. 3) shows a low soluble fraction (5.6 wt %) at 28 °C, slightly higher than that of iPP$_l$ [30], proving that only iPP glass transition is observed in DSC. The limitation of DSC implies that the thermal features of minority components at low concentrations (i.e., EPR elastomeric domains) cannot be observed. At around 95 °C, a small peak is displayed that could be matched with chains containing EP copolymers with long ethylene sequences, mentioned above, with the capability to crystallize because of the high temperature, in agreement with DSC measurement, in which a slight endotherm at around 122 °C is also identified in the thermogram related to these sequences, and matching well with the low ethylene content seen via NMR analysis. Finally, an intense peak at about 122 °C may be unequivocally assigned to iPP chains with high molecular weight, synthesized in the liquid-phase step, since it is also observed in the iPP$_l$ homopolymer in TREF and DSC analysis.

SEM measurements were performed to determine the morphology of the IPC resins. Fig. 5a and b show SEM images of the surface of the IPC resin, iPP$_l$-4E$_g$, after etching. The amorphous components, present as dispersed domains and cavities embedded into the iPP matrix, are negligible or rarely observed in this sample. Finally—and in agreement with the NMR, GPC, TREF, DSC, and SEM results—the resistance to impact of the iPP$_l$-4E$_g$ sample measured by the Charpy strength test does not improve with respect to the PP homopolymer.

3.2. *Effect of hydrogen addition on IPC*

In this section, different modifications of the sample iPP$_l$-4E$_g$ have been proposed—first, the addition of hydrogen for controlling the molecular weight; and second, the feeding of a 50/50 (v/v) mixture of propylene/ethylene monomers. The addition of hydrogen to the reactor during the first stage was fixed at a pressure of 1.0 bars, and the ethylene/propylene comonomers were fed to the same reactor during the second step, as depicted in Fig. 1b. The reaction time for this step was fixed at 4 min [30,31].

The ethylene content incorporation is rather limited (4.5 mol%) because the addition of hydrogen during synthesis increases the iPP homopolymerization at the expense of catalytic site deactivation for ethylene copolymerization [30]. However, the ethylene units are unevenly distributed with respect to the iPP$_l$-4E$_g$ sample. Thus, 1.8 mol% is dispersed across the matrix as random ethylene/propylene chains (EPE + PEP triads), and the rest (2.6 mol%) was inserted heterogeneously (EEE triad), as reflected in Table 1. As might be expected, the molecular weight for iPP$_l$-1.0-4EP$_g$ remarkably decreased (Table 1), and as with the sample iPP$_l$-4E$_g$, the ethylene units were also incorporated in the long molecules (Fig. 2).

The TREF thermogram of iPP$_l$-1.0-4EP$_g$ (Fig. 3) exhibits a similar profile to that of the iPP matrix synthesized with hydrogen in the liquid-phase stage [30,37]. This highlights the higher intensity of the shoulder near 110 °C, assigned to the presence of short PP chains as a consequence of the addition of hydrogen, which acts as a chain transfer agent.

The melting endotherm of iPP$_l$-1.0-4EP$_g$, displayed in Fig. 4, is similar to that of iPP$_l$-4E$_g$, in which a dominating peak of around 160 °C is assigned to melt the iPP crystallites, along with a small peak of around 119 °C given the limited amount of incorporated long ethylene sequences (EEE triads). Glass transition displacement is observed at a lower temperature, with regard to iPP$_l$-4E$_g$ resin, which may be due to the lower PP chains' length. The glass transition temperature associated with the EPR fraction (EPE + PEP triad) is practically undetectable, as is the case in TREF measurement, in which a rise in the soluble fraction area is not perceivable. Furthermore, the exhibited high crystallinity, very close to the iPP$_l$-4E$_g$ value (around 55%), corroborates the low ethylene incorporation.

Fig. 5e and 5f provide SEM micrographs of iPP$_l$-1.0-4EP$_g$. The images show the presence of a large number of spherical voids surrounding the amorphous EPR fraction with extremely regular size distribution. These domains are also randomly distributed throughout the iPP matrix. Despite these satisfactory morphological results and the presence of an EPR component embedded into the iPP matrix, low molecular weight impedes this resin from being ranked as an adequate IPC material. As expected, this sample shows a remarkably low value of the Charpy impact strength test (1.79 ± 0.67 kJ·m^{-2}).

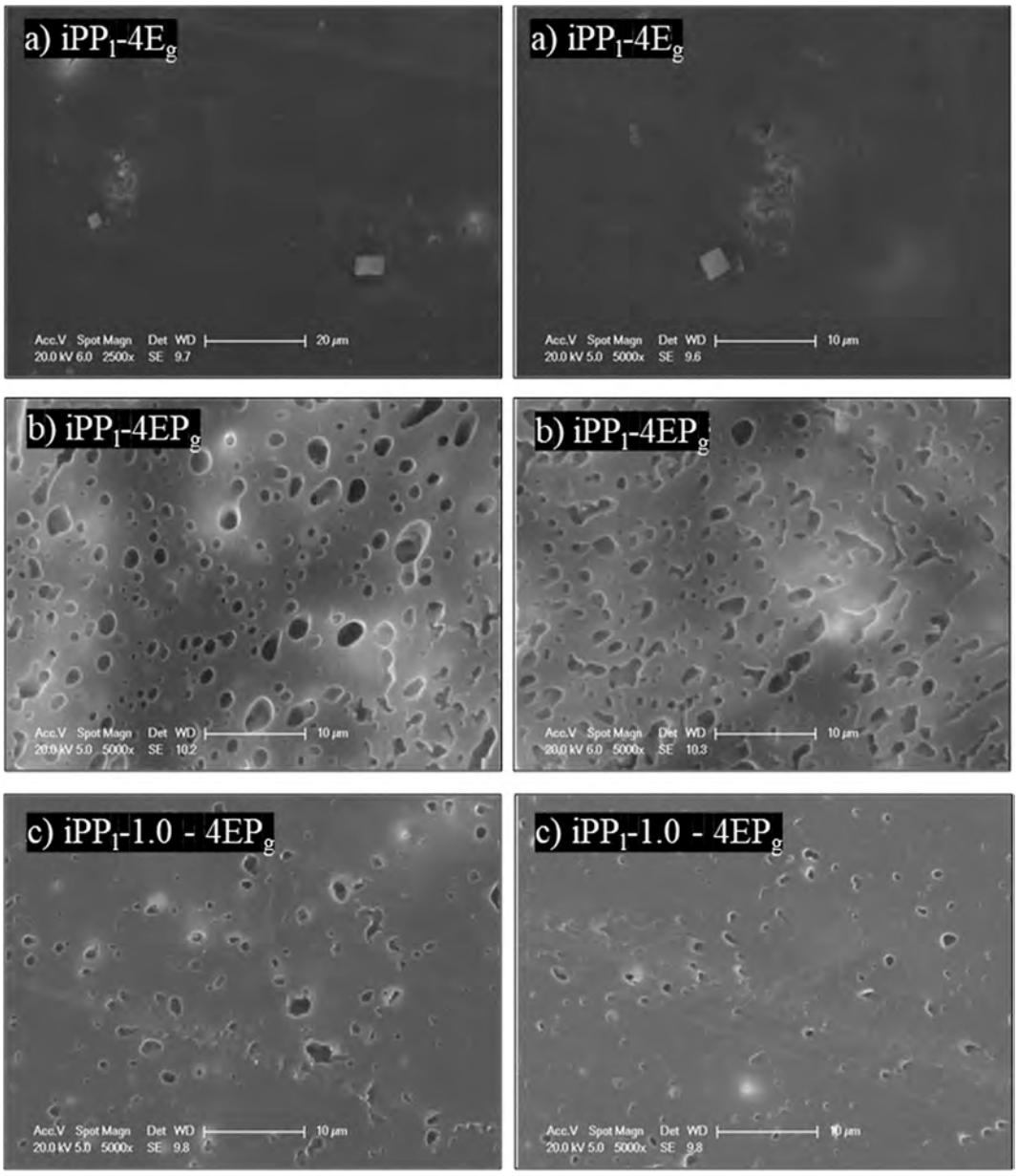

Fig. 5. SEM micrographs of IPC resins: (a) iPP$_I$-4E$_g$; (b) iPP$_I$-4EP$_g$; and (c) iPP$_I$–1.0–4EP$_g$.

3.3. Synthesis of IPC in hydrogen absence

Experimental conditions at the first and second steps clearly affect the molecular, thermal, and mechanical properties of the synthesized material, as the above results have demonstrated—(i) hydrogen addition led to a material with low molecular weight; (ii) 100 v/v% ethylene fed as the only monomer neither improved its incorporation into the polymer nor produced proper homogeneous distribution, so basically, no EPR domains were formed; and (iii) the addition of a 50/50 (v/v%) propylene/ethylene enhanced ethylene incorporation embedded in the iPP matrix with adequate homogeneous and heterogeneous ethylene distribution and, as a consequence, increased the presence of numerous amorphous EPR domains, which is a prerequisite condition to enhance impact properties and stiffness.

Accordingly, a new polymerization sequence is examined in hydrogen absence at the first step, and a 50/50 propylene-ethylene comonomer mixture is added at the second stage, in accordance with the procedure shown in Fig. 1b, to obtain the sample iPP$_I$-4EP$_g$. The lack of hydrogen generates a resin with an MWD not too wide and located at high MW values, as shown in Fig. 2 and Table 1. The variation of the content of methyl branches with molar mass is also depicted in Fig. 2. It is worth noting that the iPP$_I$-4EP$_g$ material presents lower content of methyl groups of the synthesized IPC resins. This can be attributed to the fact that higher ethylene content is incorporated in the PP matrix. Furthermore, the ethylene comonomer is preferentially incorporated in the higher molar mass molecules (>500 kg·mol^{-1}), which agrees well with the abrupt decrease of methyl branch content as MW grows, while the maximum of 250 CH_3/1,000C remains constant for lower molecular weights.

In addition, ^{13}C NMR liquid-state analysis (Table 1) confirms the remarkable increase of ethylene content incorporation (21.2 mol%) into the matrix. Moreover, ethylene is more heterogeneously than randomly distributed—12.2 mol% vs. 6.3 mol%, respectively. By comparing these values with those obtained for other HIPPs with different molecular weights, one observes a ratio between EEE and EPE + PEP triads between 1.0 and 2.0 [30,37,38,39]. All the tested materials that meet this criterion present adequate resistance to impact as required for IPC materials. Accordingly, Table 1 shows that the sample iPP$_I$-4EP$_g$ has the

best impact resistance measured by the Charpy test.

Fig. 3 displays the chemical composition distribution (CCD) of iPP_l-$4EP_g$, determined from TREF measurements. In this case, four different regions can be defined with the variation of crystallization temperatures. The peak at 28 °C is the soluble fraction that can be assigned to two contributions: the atactic fraction of the PP matrix and the EPR domains from the elastomeric phase. This result is supported by the difference in the peak intensity observed with respect to the analysis of the PP homopolymer resin, iPP_l, synthesized in the liquid-phase stage. The soluble fraction of homopolymer iPP_l, assigned to the atactic region, depicts 2.3 wt%, while the contribution of this soluble fraction in the iPP_l-$4EP_g$ copolymer represents a 35.4 wt%, and therefore, most parts can be ascribed to the amorphous elastomeric domains (EPE + PEP triads). Unlike the other IPC resins, this EPR elastomeric contribution is also observed in the DSC melting thermogram (Fig. 4) as a glass transition, located at −56.3 °C, which confirms its formation. In the second region, in the range between 30 °C and 90 °C, a broad signal corresponds to crystallizable sequences with different levels of comonomer distribution as well as ethylene, propylene, and/or EP segmented copolymers. In the third region, at 95 °C, a small peak appears that could be assigned to relatively long ethylene sequences with the capability to crystallize, matching well with the ^{13}C NMR results shown in Table 1 and with the hump at 119.3 °C detected via DSC. In the fourth region, the presence of an intense peak at about 122 °C is assigned to iPP crystallites, in agreement with the intense melting signal at 162.8 °C provided via DSC.

Fig. 5 shows the SEM micrographs of the etching cut surface of the iPP_l-$4EP_g$ sample. Dark areas are assigned to elastomeric EPR, present as homogeneous domains dispersed along the iPP matrix. The number of cavities is remarkably higher than those of the other IPC samples studied in this work given the higher ethylene content, particularly the random EP segments. These EPR domains present a predominantly circular morphology with diameters from 1 to 3 μm, which leads to a decrease in the gap of the cavities, enabling enhanced compatibility by lowering the interfacial tension of the dispersed phase against the matrix [40,41]. This indicates that random sequences might act as flexible molecules that make different components in this resin compatible, increasing mechanical resistance and proving that this is a key factor in the toughness–stiffness balance of IPC in-reactor alloys in situ. All these results explain the excellent value of Charpy impact resistance of 13.83 $kJ{\cdot}m^{-2}$ shown by the sample iPP_l-$4EP_g$, very similar to those obtained for commercial high molar mass PP impact copolymers.

3.4. Fractionation of iPP_l-$4EP_g$

To obtain more detailed information on the microstructure of iPP_l-$4EP_g$, preparative TREF was performed to fractionate the individual components. Therefore, this IPC copolymer was divided into three fractions: F1, F2, and F3, at temperatures of 50 °C, 100 °C, and 130 °C, respectively, based on the different regions observed in the corresponding analytical TREF thermogram curve of the raw iPP_l-$4EP_g$ shown in Fig. 3. The weight fraction distributions collected for these fractions are registered in Table 2. The different fractions were also analyzed via GPC-IR5, analytical TREF, and DSC.

Fig. 6a reveals the TREF profiles of the three fractions of iPP_l-$4EP_g$. As expected, peaks associated with crystalline regions appeared at higher temperatures with the increase of the fractionation temperature. F1 represents the majority of the soluble component, which includes the atactic PP and the elastomeric EPR phase. F2 showed an almost negligible multimodal broad signal assigned mainly to intermediate crystallizable EP copolymers. Moreover, this fraction contains a part of the soluble fraction as noticed by a peak at 30 °C. Finally, F3 shows bimodal compositional distribution. A peak at 115 °C clearly matches the iPP chains with higher molecular weight, and a peak at around 110 °C corresponds to the co-crystallization phenomenon of a minority iPP component with lower molecular weight.

Fig. 6b shows the second melting DSC curves for the fractions of the sample iPP_l-$4EP_g$. In F1, one can only possible observe one glass transition temperature at − 51.9 °C, which is associated with the EPR incorporated into the iPP matrix. F2 displays several melting peaks; the most intense are placed at 120.3 °C, 153.1 °C, and 160.2 °C. The peak at 120.3 °C could be assigned to EP segments with long crystallizable ethylene sequences, and the peaks at 153.1 °C and 160.2 °C, which may be related to each other via recrystallization [42], are associated with crystallizable propylene sequences with either molecular weight or isotactic index lower than the iPP matrix. F3 presents a sharp and predominant peak at 161.7 °C assigned to the iPP matrix with higher molecular weight.

Fig. 6c exhibits the MWD of the three fractions of the iPP_l-$4EP_g$ resin. The fractions of the iPP_l-$4EP_g$ copolymer have similar MWD shapes, distinguishing a fraction of high molecular weight associated with the PP matrix and the presence of an EPR fraction with high molecular mass that clearly provides remarkable impact on the strength and toughness of this resin [30,31,39,43,44,45].

Fig. 6c also shows the methyl group distribution (associated with the propylene comonomer) for the different fractions of iPP_l-$4EP_g$. Referencing the maximum number of methyl branches for each molecular weight—around 400 CH_3/1000C, as shown in Fig. 2 for iPP_l—one can determine the methyl content distribution for each fraction [31]. In F3, the methyl group number remains constant through the MWD being equivalent to the aforementioned value of the PP matrix; as a consequence, this fraction is unambiguously composed of large iPP chains associated with the PP matrix. F1, associated with a soluble fraction and composed mainly of an EP random copolymer (EPR), contains approximately 180 CH_3/1000C, the half-content with respect to the reference value, confirming the amorphous elastomeric EPR phase. It must be pointed out that methyl groups decrease smoothly from low to high molar masses. Finally, in F2, the methyl group distribution experiments a sharp decline as the molecular weight increases, from 95% to 20% of methyl groups, which confirm its heterogeneous arrangement, composed of propylene segments and propylene-ethylene chains, together with long ethylene segments, as reflected in the results obtained via TREF and DSC.

The crystalline EP segments could perform as compatibilizing agents between the two main phases of amorphous EPR and crystalline iPP [38,46]. This fact, coupled with the remarkably high molecular weight presented by the EPs' segments, allows one to improve the impact strength of this material over the iPP_l resin, leading to comparable values for commercial IPCs with similar molecular weight [47].

Table 2
Characterization results of fractions of iPP_l-$1EP_g$ material.

Sample	Fraction	wt-fraction[a](wt-%)	T_m[b] (°C)	T_g[b] (°C)	Crystallinity[b] (%)	T_e[c] (°C)
iPP_l-$4EP_g$	F1	24.1	–	−51.9	–	30
	F2	16.3	120.3/153.1/160.2	−52.0/-6.9	45.5	30/72.1/78.2/94.7/104.5
	F3	59.6	161.7	−18.7	56.1	110/115

[a] Weight fraction for the fractions collected from preparative-TREF.
[b] From second heating scanning.
[c] Elution temperature obtained by TREF.

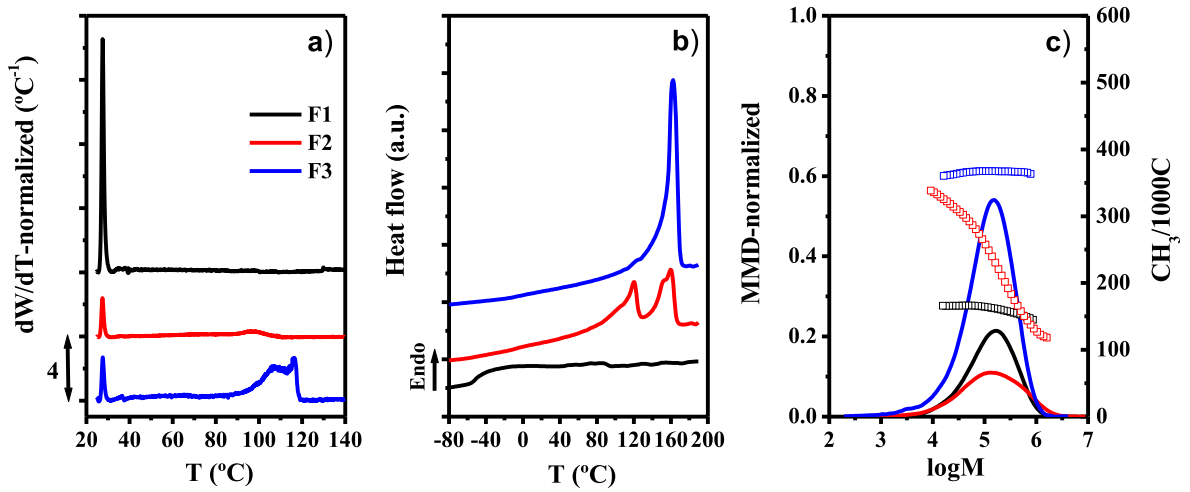

Fig. 6. (a) Normalized crystallinity distributions obtained by TREF, (b) melting thermograms, and (c) molecular weight distributions and number of methyl groups of iPP_l-$4EP_g$ fractions.

3.5. Comparison between Gas–Gas-, Liquid–Liquid-, and Liquid–Gas-Phase Two-Step IPCs (iPP_g-$1EPR_g$, PP_l-$1E_l$, and iPP_l-$4EP_g$)

Beyond the individual molecular characterization and properties of the PP copolymers synthesized in only one reactor following two different steps—liquid–liquid [30], gas–gas [31], and liquid–gas—this section summarizes and compares the main features of the PP copolymers that can be considered as IPCs.

The sample iPP_g-$1EPR_g$, with an ethylene content of 19.6 mol% and Charpy impact of 4.5 kJ·m^{-2}, was synthesized in sequential gas–gas-phase two steps, feeding in the second phase ethylene/propylene monomers in a ratio of 50/50 for 1 min. The sample PP_l-$1E_l$ (4.8 mol% ethylene; 13.56 kJ·m^{-2}) was synthesized in two sequential liquid-–liquid-phase steps, adding in the second stage ethylene monomer for 1 min. The sample iPP_l-$4EP_g$ (21.2 mol% ethylene; 13.83 kJ·m^{-2}) has been obtained in two sequential liquid- and gas-phase steps, adding a 50/50 (v/v) mixture of propylene/ethylene monomers for 4 min in the second phase. Such differences in synthesis procedures are reflected in similarities and differences among these three copolymers. However, considering that the impact resistance of PP copolymers synthesized in the gas–gas phase is three times lower than that of IPC copolymers synthesized in the liquid–liquid and liquid–gas phases, respectively, far from the value required to be considered as an IPC resin, the comparative study has focused on the last two IPC copolymers that have similar impact resistance.

The copolymer particle morphology has been observed via SEM (Fig. 7). The micrographs show that both resins are composed of particles with a spherical morphology that, in some cases, are interconnected to form agglomerates, especially in iPP_l-$4EP_g$. The average size of the particles has been estimated by cross-sectional area using imaging analysis to get an average area of 0.37 mm^2 and 0.21 mm^2 for PP_l-$1E_l$ and iPP_l-$4EP_g$, respectively. This difference in size is because elastomeric component (EPR) diffusion in the liquid-phase stage is the most favored, so average particle size is also larger. Higher magnification images of the particle surface show the presence of fibrils with a gummy appearance attributed to the elastomeric phase since these were not observed on the surface of the iPP homopolymer particle [29]. These fibrils are more numerous in iPP_l-$4EP_g$.

Fig. 8 shows the SEM micrographs of the etching cut surface of both copolymers. In these images, the dark cavities are assigned to elastomeric EPR, and these areas are homogeneously dispersed along the iPP matrix in both samples, which results in enhanced compatibility between the two main phases of amorphous EPR and crystalline iPP, reflected in the similar high-impact-resistant values of 13.6 kJ·m^{-2} and

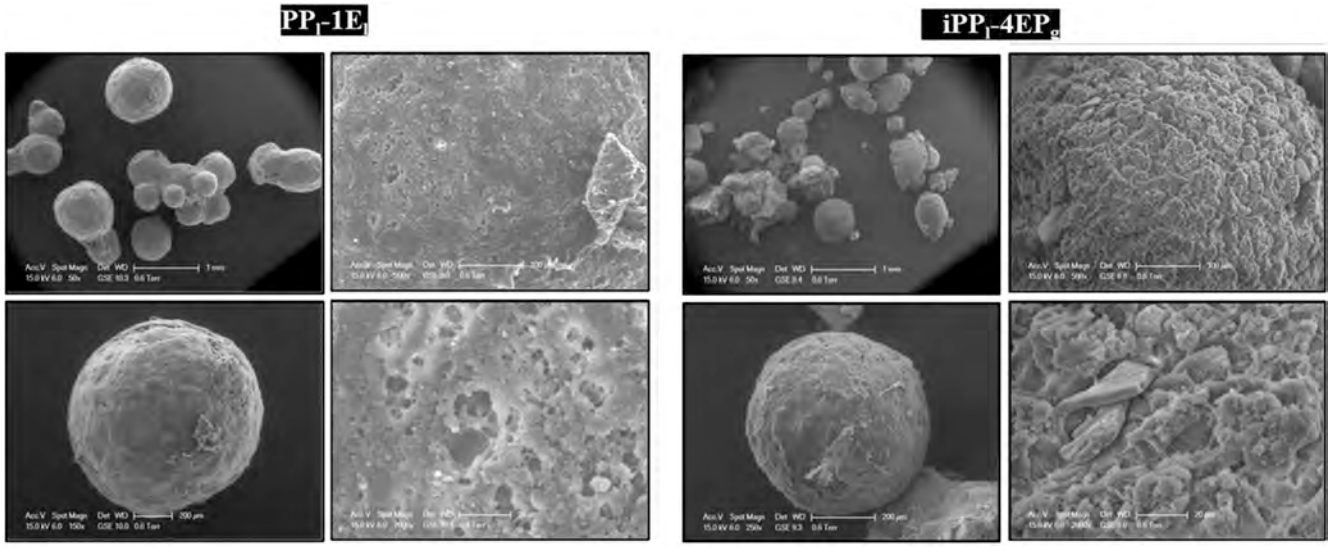

Fig. 7. SEM micrographs of particles corresponding to PP_l-$1E_l$ and iPP_l-$4EP_g$.

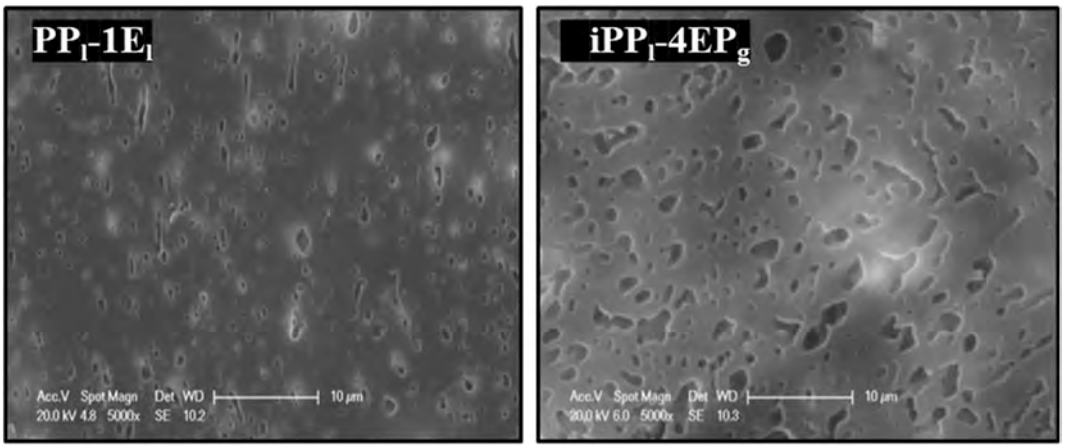

Fig. 8. SEM micrographs of cut surfaces corresponding to PP$_l$-1E$_l$ and iPP$_l$-4EP$_g$.

13.8 kJ·m^{-2} present in both samples.

To this day, separate information on the molar mass distribution and CCD of IPC resins has been obtained via SEC and TREF. To provide more information about the molecular structure for a more comprehensive characterization of these complex IPC materials, two-dimensional distribution interrelating molar mass and chemical composition is determined by means of CFC [48,49]. Fig. 9a and 9b show the bivariate distribution of the samples PP$_l$-1E$_l$ and iPP$_l$-4EP$_g$. In general, both plots show two well-differentiated contributions, the amorphous soluble fraction at temperatures below 30 °C, and the crystalline fractions in a broad range of temperatures above 40 °C.

From the compositional point of view, both samples are quite similar in those regions eluted in the 90 °C – 100 °C and 100 °C–125 °C ranges, which are associated with chains based on long ethylene molecules or long propylene chains, respectively. However, between 75 °C and 90 °C, the tridimensional surface plot of sample iPP$_l$-4EP$_g$ reveals areas of clearly distinct positions in the molar mass/chemical composition plane shifted to high molar mass molecules, mainly at 85 °C–90 °C, compared with those observed for sample PP$_l$-1E$_l$, which can be associated with various copolymers composed by extended ethylene and propylene

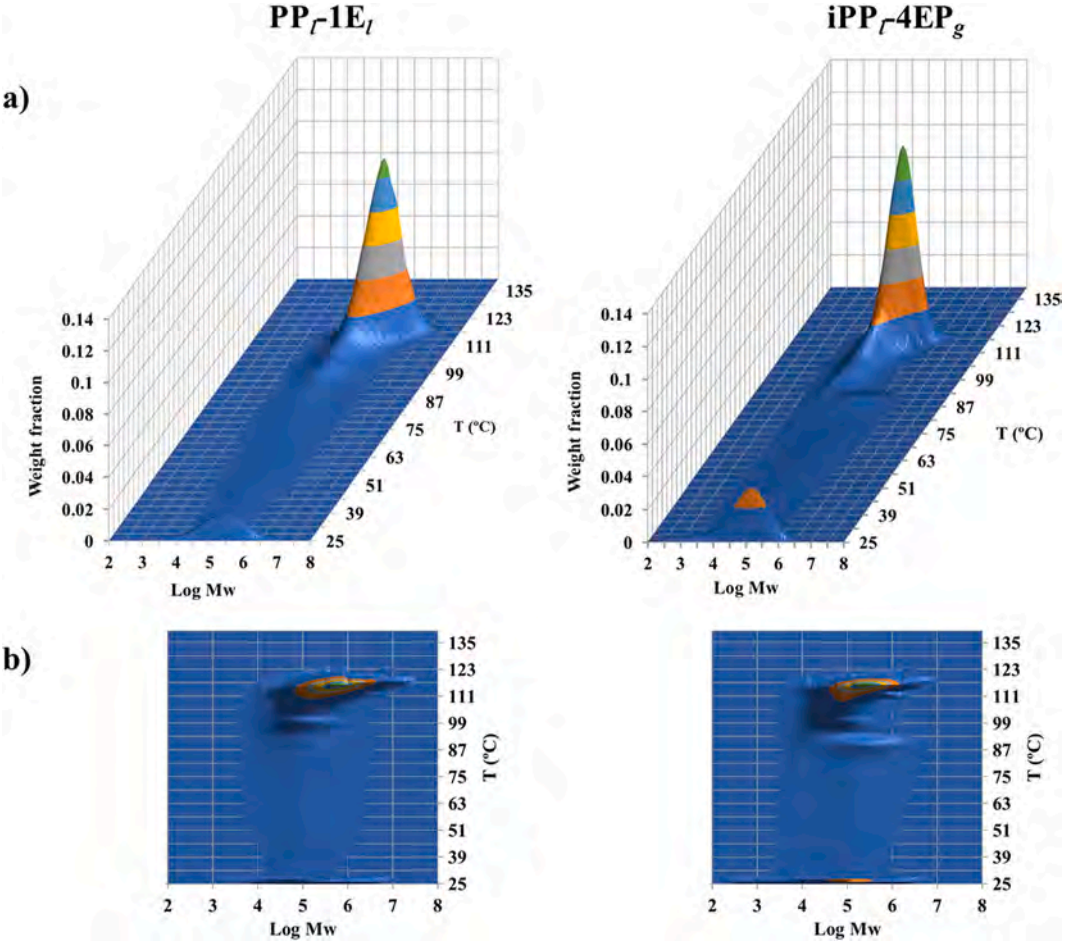

Fig. 9. a) 3D-CFC and b) 2D-contour of samples PP$_l$-1E$_l$ and iPP$_l$-4EP$_g$.

copolymer (EP) sequences.

Fig. 10 displays the CFC bidimensional plot from the molar mass point for both samples. In general, all the iPP_l-$1E_l$ fractions show a higher molecular weight than the iPP_l-$4EP_g$ ones except for those fractions eluted in the range from 75 °C to 90 °C whose molar masses are lower (at 75 °C) than those of the iPP_l-$4EP_g$ fractions.

Bearing in mind that the molar mass of whole iPP_l-$4EP_g$ is lower than that of whole iPP_l-$1E_l$, one would expect that its impact resistance should also be lower, in agreement with the influence of the molecular weight on the impact strength, but rather, the opposite is the case. A possible explanation for this finding could be the great compatibilizing effect between the iPP matrix and the rubber phase supplied by the high-molecular-weight EP segments eluted at 85 °C–90 °C [42], together with the increased overall ethylene content in the material (21% mol) and the right balance between EEE and EPE + PEP heterogeneous and homogeneous segment distributions.

4. Conclusions

For the synthesis of IPC in two sequential steps in different phases (liquid and gas) in a single reactor, changes have been made in the process synthesis. When the feeding process at the second step consisted solely of ethylene, the impact resistance of the polymer was similar to that of the PP homopolymer. When hydrogen was added during the reaction, in the first step, the molecular weight of the copolymer obtained was too low, and consequently, its impact resistance was also too low. Finally, an IPC material with impact resistance like that of commercial PP impact copolymers with a good distribution of the elastomeric phase was achieved in a single reactor following a liquid- and gas-phase sequential process in hydrogen absence and the addition of a 50/50 (v/v) mixture of propylene/ethylene monomers. The IPC so obtained exhibited a good distribution of the elastomeric EPR phase in the PP matrix in size and number.

It was also determined that the ratio between EEE and EPE + PEP triads ranging from 1.0 and 2.0 is a good criterion to predict the proper impact resistance of any heterophasic PP copolymer in-reactor alloy.

Preparative TREF fractionation and subsequent fraction characterization via DSC and GPC-IR5 as well as SEM characterization of the surface of the IPCs proved that the adequate ratio between the continuous iPP phase and the elastomeric domains of EPR dispersed phases is the key to provide a good balance between toughness and stiffness.

Finally, from the comparison of the IPCs synthesized in only one reactor following two different steps (liquid–liquid, gas–gas, and liquid–gas) and in the absence of hydrogen, considering impact resistance, the values of impact strength of the IPC copolymers synthesized in the gas–gas phase were three times lower than those of the IPC copolymers synthesized in the liquid–liquid and liquid–gas phases, respectively.

The use of the CFC (bivariate TREF-GPC distribution) technique allowed a comparison of the liquid–liquid- and liquid–gas-phase IPC copolymers and highlighted that although both materials presented similar CCD, they presented remarkable differences in terms of molar mass distribution. Thus, while the liquid–gas-phase IPC material showed generally lower molecular weight than the liquid–liquid-phase IPC, the presence of a region of crystalline families eluted between 85 °C and 90 °C composed of high molecular weight and attributed to EP copolymers suggests that this can act as a compatibilizing agent between the iPP matrix and the rubber phase, allowing one to improve its impact resistance and equaling, even slightly exceeding, that of the liquid–liquid-phase IPC copolymer. Considering these results, the synthesis of IPC resins in a single reactor is an efficient experimental method for research on PP impact copolymers.

Funding

This research received no external funding.

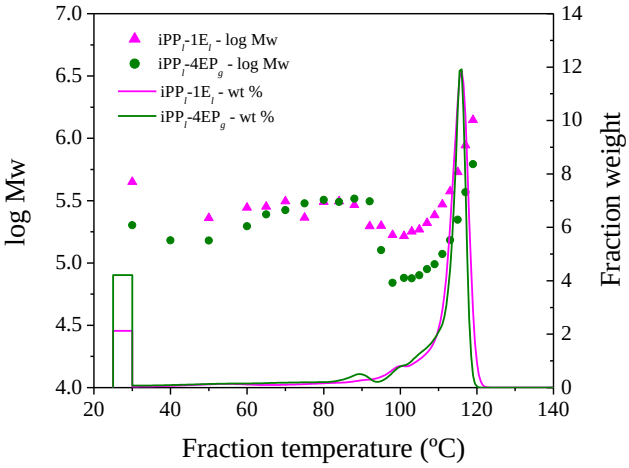

Fig. 10. 2D-CFC of samples PP_l-$1E_l$ and iPP_l-$4EP_g$.

CRediT authorship contribution statement

María Teresa Pastor-García: Investigation. **Inmaculada Suárez:** Investigation, Writing - review & editing. **María Teresa Expósito:** Investigation, Writing - original draft. **Baudilio Coto:** Supervision, Writing - review & editing. **Rafael A. García-Muñoz:** Supervision, Conceptualization, Writing - review & editing, Funding acquisition.

Declaration of Competing Interest

The authors declare that they have no known competing financial interests or personal relationships that could have appeared to influence the work reported in this paper.

Acknowledgments

The authors are kindly acknowledged to Polymer Technology Laboratory (LATEP) from Rey Juan Carlos University for the ethylene-propylene copolymers characterization.

Data availability

The raw/processed data required to reproduce these findings cannot be shared at this time as the data also forms part of an ongoing study.

References

[1] J. Chen, J. Kang, J. Yang, S. Zhu, F. Yang, Y. Cao, M. Xiang, H. Li, Controlled properties of high-impact polypropylene in-reactor alloys by tailoring chemical structure and morphology, Journal of Polymer Research. 22 (180) (2015) 1–8.
[2] C. Chen, Designing catalysts for olefin polymerization and copolymerization: beyond electronic and steric tuning, Nature Reviews Chemistry. 2 (2018) 6–14.
[3] F. Chen, B. Qiu, Y. Shangguan, Y. Song, Q. Zheng, Correlation between impact properties and phase structure in impact polypropylene copolymer, Materials and Design 69 (2015) 56–63.
[4] Y.S. Thio, A.S. Argon, R.E. Cohen, M. Weinberg, Toughening of Isotactic Polypropylene with $CaCO_3$ Particles, Polymer 43 (2002) 3661–3674.
[5] Y. Chen, Y. Chen, W. Chen, D. Yang, Morphology of high impact polypropylene particles, Polymer 47 (2006) 6808–6813.
[6] J. Debling, W. Harmonray, Morphological development to Impact Polypropylene Produced in Gas Phase with a $TiCl_4/MgCl_2$ Catalyst, Journal of Applied Polymer Science 81 (2001) 3085–3106.
[7] E. Jia, S. Zhao, Y. Shangguan, Q. Zheng Toughening mechanism of polypropylene bends with polymer particles in core-shell structure: equivalent rubber content effect related to core-shell interfacial strength. Polymer, 178 (2019), 121602.
[8] L. Santonja-Blasco, W. Rungswang, R.G. Alamo, Influence of Chain Microstructure on Liquid-Liquid Phase Structure and Crystallization of Dual Reactor Ziegler-Natta Made Impact Propylene-Ethylene Copolymers, Industrial and Engineering Chemistry Research 56 (12) (2017) 3270–3282.
[9] M. Gahleitner, C. Tranninger, P. Doshev, Heterophasic Copolymers of Polypropylene: Development, Design Principles, and Future Challenges, Journal of Applied Polymer Science 130 (2013) 3028–3037.

[10] M. Daftaribesheli, Thesis: Comparison of catalytic ethylene polymerization in slurry and gas phase, University of Twente-The, Netherlands Eindhoven, 2009.
[11] T. Xie, K.B. McAuley, J.C.C. Hsu, D.W. Bacon, Gas phase ethylene polymerization: production processes, polymer properties, and reactor modeling, Industrial and Engineering Chemistry Research 33 (1994) 449–479.
[12] Optimized Ziegler-Natta Catalysts for Gas Phase PP Processes. https://www.lyondellbasell.com/globalassets/products-technology/technology/gas-phase-pp-processes.pdf?id=13744, 2015 (accessed 16 April 2021).
[13] H.A. Maddah, Polypropylene as a Promising Plastic: A Review, American Journal of Polymer Science 6 (1) (2016) 1–11.
[14] W. Liu, J. Zhang, M. Hong, P. Li, Y. Xue, Q. Chen, X. Ji, Chain microstructure of two highly impact polypropylene resins with good balance between stiffness and toughness, Polymer 188 (2020) 1221462020.
[15] C. Li, Z. Wang, W. Liu, X. Ji, Z. Su, Copolymer Distribution in Core-Shell Rubber Particles in High-Impact Polypropylene Investigated by Atomic Force Microscopy-Infrared, Macromolecules 53 (7) (2020) 2686–2693.
[16] F. Li, Y. Gao, C. Zhang, J. Jin, X. Ji, Y. Zhang, X. Zhang, W. Jiang, Design of high impact thermal plastic polymer composites with balanced toughness and rigidity: Effect of matrix polymer molecular weight, Polymer 201 (2020), 122957.
[17] F. Li, Y. Gao, Y. Zhang, W. Jiang, Design of High Impact Thermal Plastic Polymer Composites with Balanced Toughness and Rigidity: Toughening with Core-Shell Rubber Modifier, Polymer 191 (2020), 122237.
[18] L. Jeremic, A. Albrecht, M. Sandholzer, M. Gahleitner, Rapid characterization of high-impact ethylene–propylene copolymer composition by crystallization extraction separation: comparability to standard separation methods, International Journal of Polymer Analysis and Characterization 25 (8) (2020) 581–596.
[19] W. Dengfei, W. Jian, G. Feng, G. Yuxin, D. Wei, Y. Guoxing, Progress in technology and catalysts for gas phase polyethylene processes, Advances in Sciences and Engineering 8 (1) (2016) 25–31.
[20] A. Watson, B. Fajardo, T. Gormanos, M. Gahleitner, J. Wang, H. Braun, F. Bergfors, Tube made of a heterophasic polypropylene composition. (U.S. Patent No. 2018/0201756 A1) (2018).
[21] M. Gahleitner, J. Wang, F. Berger, J. Lilja, Heterophasic polypropylene composition with improved mechanical and optical properties. (U.S. Patent No. 2020/0048443 A1) (2020).
[22] M. Sandholze, C. Tranninger, J. Wang, M. Gahleitner, Heterophasic polypropylene composition with improved mechanical and optical properties. (U.S. Patent No. 10,907,036 B2) (2021).
[23] R. A. Meyers. Handbook of petrochemicals production processes. Chapter 16.1: Basell Spheripol Technology for PP Production. M. Dorini, G. ten Berge, Mc Graw-Hill (2005).
[24] I. Urdampilleta, A. González, J.J. Iruin, J.C. de la Cal, J.M. Asua, Origins of Product Heterogeneity in the Spheripol High Impact Polypropylene Process, Ind. Eng. Chem. Res. 45 (2006) 4178–4187.
[25] Z. Fan, Y. Zhang, J. Xu, H. Wang, L. Feng, Structure and properties of polypropylene/poly(ethylene-co-propylene) in-situ blends synthesized by spherical Ziegler-Natta catalyst, Polymer 42 (2001) 5559–5566.
[26] Z. Fu, S. Tu, Z. Fan, Effect of the Combined External Electron Donors on the Structure and Properties of Polypropylene/Poly(ethylene-co-propylene) In-Reactor Alloys Prepared by High-Efficiency Industrial Ziegler-Natta Catalyst, Ind. Eng. Chem. Res. 52 (2013) 5887–5894.
[27] B. Zhang, Z. Fu, Z. Fan, P. Phiriyawirut, S. Charoenchaidet, Preparation and characterization of high MFR polypropylene and polypropylene/poly(ethylene-co-propylene) in-reactor alloys, J. Appl. Polym. Sci. 133 (8) (2016) 42984.
[28] J. J. McKetta Jr. Polypropylene, Gas-Phase Process. Encyclopedia of Chemical Processing and Design: Polypropylene Gas Phase Process, Marcel Dekker Inc., New York, 1992, pp. 77–89.
[29] C. Jiang, B. Jiang, Y. Yang, Z. Huang, Z. Liao, J. Sun, J. Wang, Y. Yang, Enhanced multiphase interfacial interaction of impact polypropylene copolymer by in-situ introducing polyethylene, Polymer 214 (2021), 123373.
[30] M.T. Pastor-García, I. Suárez, M.T. Expósito, B. Coto, R.A. García-Muñoz, New method of single liquid-phase reactor synthesis of high-impact polypropylene: Structure, morphology, and impact properties of copolymers, European Polymer Journal 93 (2017) 436–447.
[31] M.T. Pastor-García, I. Suárez, M.T. Expósito, B. Coto, R.A. García-Muñoz, Influence on properties and phase structure of single gas-phase reactor made impact polypropylene copolymers, Eur. Polym. J. 106 (2018) 156–168.
[32] P. Aigner, C. Paulik, A. Krallis, V. Kanellopoulos, Optimal Catalyst and Cocatalyst Precontacting in Industrial Ethylene Copolymerization Processes, Journal of Polymers 2016 (2016) 1–10.
[33] P. Roos, G.B. Meier, J.J.C. Samson, G. Weickert, K.R. Westerterp, Gas phase polymerization of ethylene with a silica supported metallocene catalyst: influence of temperature on deactivation, Macromolecular Rapid Communications 18 (1997) 319–324.
[34] J.-M. Zhou, N.-H. Li, N.-Y. Bu, D.T. Lynch, S.E. Wanke, Gas-phase ethylene polymerization over polymer-supported metallocene catalysts, Journal of Applied Polymer Science 90 (2003) 1319–1330.
[35] J.C. Randall, Polymer sequence determination – carbon-13 NMR method, Journal of Macromolecular Science Part C Polymer Reviews 29 (1989) 201–317.
[36] M. Kakugo, Carbon-13NMR determination of monomer sequence distribution in ethylene–propylene copolymers prepared with titanium trichloride–diethylaluminum chloride, Macromolecules 15 (1982) 1150–1152.
[37] R.A. García, B. Coto, M.-T. Expósito, I. Suárez, A. Fernández, S. Caveda, Molecular Characterization of Polypropylene Heterophasic Copolymers by Fractionation Techniques, Macromolecular Research 19 (2011) 778–788.
[38] A. Fernández, M.T. Expósito, B. Peña, R. Berger, J. Shu, R. Graf, H.W. Spiess, R. García-Muñoz, Molecular structure and local dynamic in impact polypropylene copolymers studied by preparative TREF, solid state NMR spectroscopy, and SFM microscopy, Polymer 61 (2015) 87–98.
[39] A. Fernández Fernández, Thesis: Análisis de la estructura, movilidad molecular y propiedades de copolímeros de impacto de polipropileno. Modelo de estructura de fases. Universidad Rey Juan Carlos, 2014. https://burjcdigital.urjc.es/bitstream/handle/10115/12236/Tesis%20Doctoral%20Almudena%20Fern%C3%A1ndez.pdf?sequence=1&isAllowed=y (accessed 16 April 2021).
[40] J.U. Starke, G.H. Michler, W. Grellmann, S. Seidler, M. Gahleitner, J. Fiebig, E. Nezbedova, Fracture toughness of polypropylene copolymers: influence of interparticle distance and temperature, Polymer 39 (1998) 75–82.
[41] P. Doshev, R. Lach, G. Lohse, A. Heuvelsland, W. Grellmann, H.-J. Radusch, Fracture characteristics and deformation behavior of heterophasic ethylene–propylene copolymers as a function of the dispersed phase composition, Polymer 46 (2005) 9411–9422.
[42] S. Cheruthazhekatt, T.F.J. Pijpers, G.W. Harding, V.B.F. Mathot, H. Pasch, Compositional Analysis of an Impact Polypropylene Copolymer by Fast Scanning DSC and FTIR of TREF-SEC Cross-Fractions, Macromolecules 45 (2012) 5866–5880.
[43] H. Tan, L. Li, Z. Chen, Y. Song, Q. Zheng, Phase morphology and impact toughness of impact polypropylene copolymer, Polymer 46 (2005) 3522–3527.
[44] Q. Dong, X. Wang, Z. Fu, J. Xu, Z. Fan, Regulation of morphology and mechanical properties of polypropylene/poly(ethylene-co-propylene) in-reactor alloys by multi-stage sequential polymerization, Polymer 48 (2007) 5905–5916.
[45] H.J. Radusch, P. Doshev, G. Lohse, Phase behavior and mechanical properties of heterophasic polypropylene—ethylene/propylene copolymers systems, Polymer 50 (2005) 279–285.
[46] L. Santonja-Blasco, W. Rungswang, R.G. Alamo, Characterization and Morphological Distribution of Ethylene Content in Impact Propylene Copolymers, Macromol. Symp. 377 (2018) 1700046–1700053.
[47] J.D. Encarnacion, S. Jun Park, Y. Soo Ko, Polymerization of heterophasic propylene copolymer with $Me_2Si(2\text{-}Me\text{-}4\text{-}PhInd)_2ZrCl_2$ supported on SiO_2 and SiO_2-$MgCl_2$ carriers, Korean J. Chem. Eng. 37 (2) (2020) 380–386.
[48] S. Liberman, A. Paula de Azeredo, F.P. Dos Santos, M.A. da Silva, B. Monrabal, N. Mayo, Poly(propylene) Heterophasic Copolymers: Molecular Structure Analysis through Fractionation Techniques, Macromol. Symp. 330 (2013) 30–41.
[49] B. Monrabal, L. Romero, Separation of Polypropylene Polymers by Crystallization and Adsorption Techniques, Macromol. Chem. Phys. 215 (2014) 1818–1828.